Taylor Dispersion Analysis to support lipidnanoparticle formulations for mRNA vaccines

Camille Malburet, Laurent Leclercq, Jean-François Cotte, Jérôme Thiebaud, Emilie Bazin, Marie Garinot, Hervé Cottet

Taylor dispersion analysis to support LNP formulations for mRNA vaccines

Camille Malburet[1,2], Laurent Leclercq[1], Jean-François Cotte[2], Jérôme Thiebaud[2], Emilie Bazin[2], Marie Garinot[2], Hervé Cottet[1*]

[1] IBMM, University of Montpellier, CNRS, ENSCM, Place Eugène Bataillon, 34090 Montpellier, France

[2] Sanofi Pasteur, Analytical Sciences, 1541 avenue Marcel Mérieux, 69280 Marcy l'Etoile, France

[*]Correspondence should be addressed to H.C. (herve.cottet@umontpellier.fr)

Short title: **TDA to support LNP formulations for mRNA vaccines**

Abstract

Lipid nanoparticles (LNPs) are currently the most advanced non-viral clinically approved messenger ribonucleic acid (mRNA) delivery systems. The ability of a mRNA vaccine to have a therapeutic effect is related to the capacity of LNPs to deliver the nucleic acid intact into cells. On the one hand, the role of LNPs is to protect mRNA, especially from degradation by ribonucleases (RNases) and, on the other hand, to allow it to access the cytoplasm of cells where it can be translated into the protein of interest. LNPs enter cells by endocytosis and their size is a critical parameter impacting cellular internalization. In this work, we studied different formulation parameters impacting LNPs size. Taylor dispersion analysis (TDA) was used to determine the LNPs size and size distribution and the results were compared with those obtained by Dynamic Light Scattering (DLS). TDA was also used to study both the degradation of mRNA in the presence of RNases and the encapsulation rate within LNPs.

Introduction

Prophylactic vaccines stimulate the immune system to produce immunity against a specific pathogen, protecting the person from future infections. Thereby, during the last century, conventional vaccine approaches have drastically reduced the mortality and morbidity associated with infectious diseases.[1,2] Despite this success, the number of untreated medical needs remains high and new infectious diseases are periodically appearing.[3] The development of new vaccine strategies is therefore required.

Messenger ribonucleic acid (mRNA) vaccines have emerged as promising and versatile alternatives to conventional vaccine approaches.[4] These vaccines do not carry any typical antigen but rather the information for producing it using the cell machinery and turning the body into its own antigen factory. This is close to the process of natural viral infections, where viral genetic information is used to produce viral proteins from within a host cell. The use of mRNA vaccine has several beneficial features over whole pathogen, subunit or DNA-based vaccines. Indeed, mRNA is a non-infectious platform that does not need to enter the cell nucleus to be effective.[5] Moreover, mRNA vaccines have the potential for rapid development and manufacturing in case of disease outbreak, thanks to high yields of *in vitro* transcription reactions and because different mRNA vaccines can be manufactured across one single platform. The first report of successful use of *in vitro* transcribed (IVT) mRNA was published in 1990, when mRNAs were injected into mice and protein production was detected.[6] However, until recently, use of mRNA vaccine has been hold back by mRNA instability, innate immunogenicity and inefficient intra cellular delivery.[7] Recent advances on IVT-mRNA structure and RNA delivery systems have allowed to overcome these issues, and mRNA vaccines now show considerable promise for both prophylactic and therapeutic vaccines.[8] Onpattro® (patisiran) was the first RNA-based drug approved by the Food and Drug Administration (FDA) and the European Medicines Agency

(EMA) in 2018.[9] This drug uses siRNAs encapsulated into lipid nanoparticles (LNPs) for the treatment of hereditary transthyretin-mediated (hATTR) amyloidosis.[10,11] Since then, other highly effective RNA-based vaccines using LNPs have been developed and approved in a record time during the COVID-19 epidemic.[12] This opens the way and the hope for the acceleration of the development of new vaccines based on mRNA vaccine technology.[13] Yet, some points still need to be optimized such as the stability of the formulations[14,15], the endosomal escape efficiency[16,17] and the precise targeting of certain organs[18–20].

LNPs are not only simple carriers, but they also play an active role in the vaccine efficacy.[21] Among other physicochemical parameters, the size of the LNPs is a critical parameter that has an important effect on their *in vivo* behavior. Particle size is known to influence the pathway of cell internalization and intracellular processing.[22–25] Size also influences the circulation times of LNPs.[26] The size of LNPs can therefore be optimized to specifically target certain organs.[27–29] Moreover, size characterization is also of major importance during stability studies as it is necessary to verify that there is no aggregation or fusion between the LNPs and that their size remains stable. It is also necessary to verify that the mRNA size does not decrease as an indication of degradation.[14] Optimizing mRNA vaccine formulations requires the development of new analytical methods to better understand the points that remain to be investigated and to challenge existing methods.

In this work, Taylor dispersion analysis (TDA) was used as a powerful tool for the optimization of LNPs formulations. LNPs of different sizes were formulated by modifying three parameters: *(i)* the PEG-lipid ratio, *(ii)* the total flow rate (TFR) and *(iii)* the flow rate ratio (FRR). The sizes and size distribution obtained were then compared to those obtained by Dynamic Light Scattering (DLS) that is a method widely used for the monitoring of LNPs

formulations.[26,30] TDA was also used to follow the degradation of mRNA in the presence of ribonucleases and to determine the encapsulation rate of mRNA within the LNPs.

Results

Nine formulations of lipid nanoparticles (LNPs) were produced by rapid dilution of an ethanolic phase containing the lipids in a citrate buffer, as shown in Figure 1. The first three formulations [F1-F3] have been formulated with mRNA contained in the citrate buffer and the next six [F4-F9] without mRNA. Three formulation parameters have been studied: *(i)* the level of PEG, *(ii)* the total flow rate and *(iii)* the flow rate ratio between the aqueous and the organic phase.

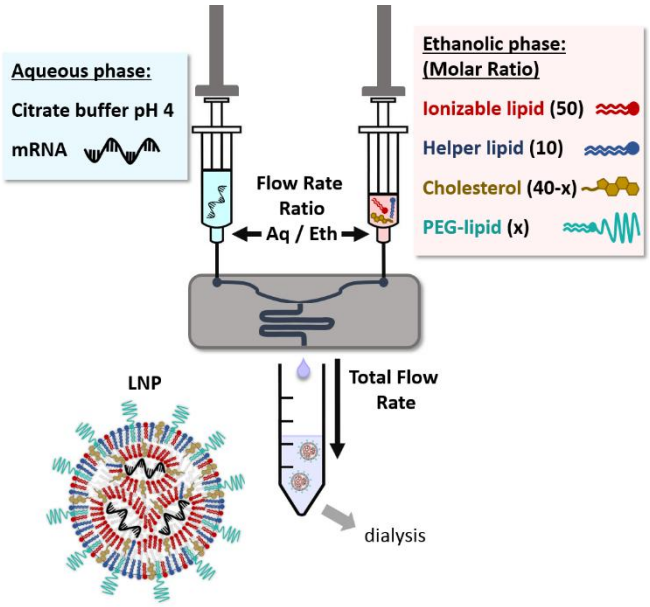

Figure 1: Schematic representation of lipid nanoparticles (LNPs) formulation by rapid dilution of an ethanolic phase containing lipids in an aqueous phase containing mRNA. At low pH, the ionizable lipids are positively charged and electrostatic interactions between the negatively charged mRNA and the ionizable lipids result in the formation of the LNPs nuclei. At the same time, hydrophobic interactions between the lipids and the aqueous phase cause the lipids to group to avoid contact with the aqueous phase resulting in the formation of the LNPs envelope.

The formulations were then analyzed in triplicates by TDA and the mean hydrodynamic diameters were calculated by fitting the elution peaks obtained (see Figure S1). Figure 2A shows that decreasing the PEG level from 5 to 0.5% led to an increase in the hydrodynamic diameters of the LNPs from 52 to 216 nm, respectively, Figure 2B shows that a decrease in the total flow rate from 6 to 1 mL/min resulted in an increase in the hydrodynamic diameters from 83 to 121 nm, respectively. Figure 2C shows that a decrease in the flow rate ratio from 5:1 to 2:1 also resulted in an increase in the hydrodynamic diameters from 79 to 100 nm, respectively.

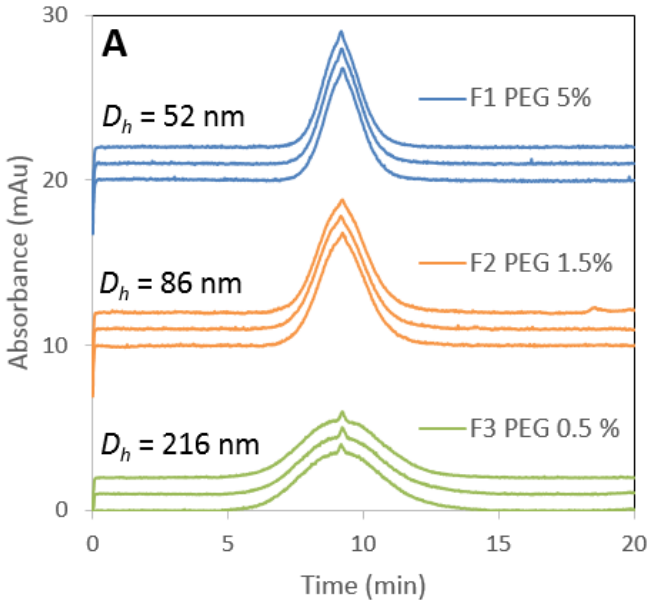

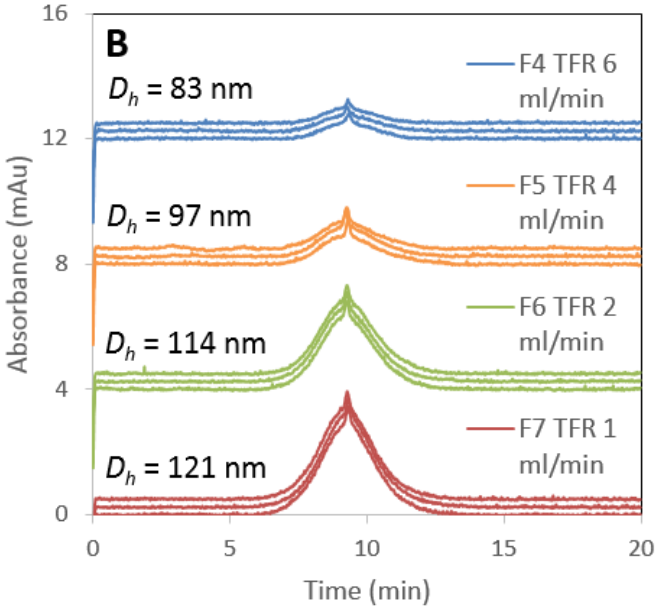

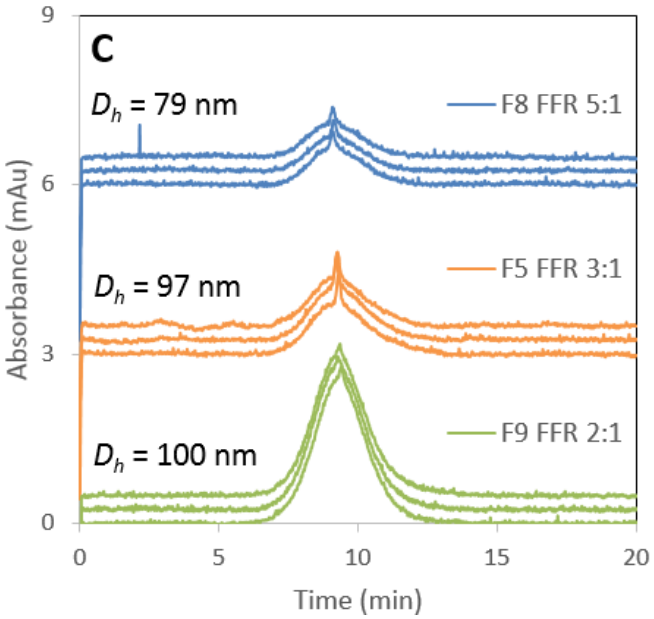

Figure 2: Taylorgrams obtained for LNPs size characterization. Impact of formulation parameters: PEG-lipid ratio (A), Total Flow Rate (TFR) (B), Flow Rate Ratio (FRR) (C). Experimental conditions: µSIL-FC coated capillaries of 61 cm total length (52.5 cm to the UV detector) × 50 µm i.d. Buffer: 10 mM PBS, pH 7.4, $\eta = 0.9\times10^{-3}$ Pa.s. Capillary presaturation: LNPs for 10 min at 60 mbar. Capillary preconditioning: H_2O for 2 min at 960 mbar followed by 2 min PBS at 960 mbar. Injection of LNPs: 20 mbar, 6 s. Mobilization pressure: 60 mbar. Sample: LNPs (DLin-MC3-DMA:DSPC:Chol:DMG-PEG-2000 at 50:10:40-x:x molar ratio) empty or encapsulating Firefly Luciferase (FLuc) mRNA. UV detection: 200 nm. Temperature: 25°C. Results presented in staggered triplicates.

The mean hydrodynamic diameters and the polydispersity indices of all LNPs formulations were also measured by DLS for comparison (see Table 1). The size distributions obtained by DLS and by TDA using Regularized Linear Inversion (CRLI) algorithm[31] were given in Figure S2 and Figure S3, respectively, and the corresponding polydispersity indexes were gathered in Table 1. The results obtained by TDA and DLS were compared and for all the LNPs formulations, the sizes and polydispersity indices obtained by TDA were systematically lower than those obtained by DLS.

Table 1: Summary of the formulation parameters of the nine studied formulations and comparison of the hydrodynamic diameters (D_h) and the polydispersity index (*PDI*) obtained by both TDA and DLS.

		F1	F2	F3	F4	F5	F6	F7	F8	F5	F9
Formulation parameters	**% PEG**	**5**	**1.5**	**0.5**	1.5	1.5	1.5	1.5	1.5	1.5	1.5
	TFR (mL/min)	4	4	4	**6**	**4**	**2**	**1**	4	4	4
	FFR	3:1	3:1	3:1	3:1	3:1	3:1	3:1	**5:1**	**3:1**	**2:1**
	mRNA	yes	yes	yes	/	/	/	/	/	/	/

Results	**D_h TDA (nm)**	52	86	216	83	97	114	121	79	97	102
	***PDI* TDA**	0.004	0.011	0.017	0.011	0.019	0.015	0.072	0.001	0.009	0.064
	D_h *DLS* (nm)	93	128	239	85	117	144	191	91	117	132
	***PDI* DLS**	0.176	0.123	0.159	0.152	0.171	0.166	0.151	0.156	0.171	0.141

Figure 3A displays the size distributions obtained by TDA for formulation F1, F3 and a 50/50 (v/v) F1-F3 mixture. Figure 3B displays the size distributions of the same samples obtained by DLS for comparison. In DLS, the size distributions of the two formulations analyzed separately were shown to overlap with [30-300] nm for F1 and [110-600] nm for F2, which was not the case in TDA ([35-70] nm for F1 and [160-280] nm for F2). When analyzing the F1-F3 mixture, a single population with a very broad peak of [30-600] nm and an average size of 211 nm was observed in DLS, while two distinct populations of [40-70] nm and [160-240] nm were observed in TDA.

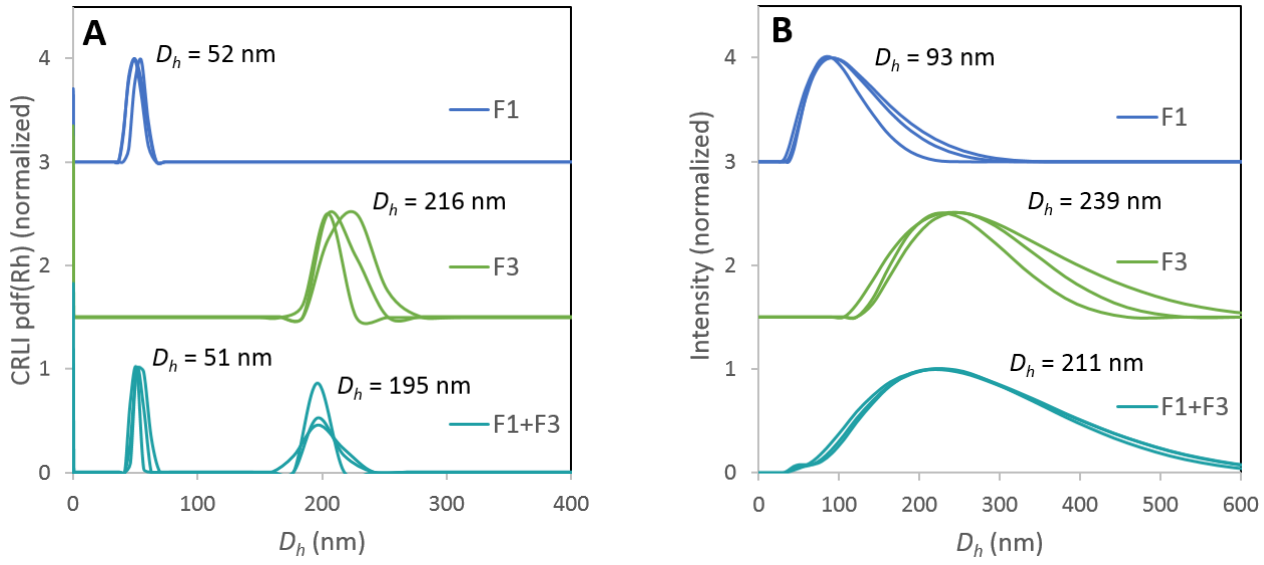

Figure 3: Size distribution obtained by TDA (A) and DLS (B) for formulation F1, F3 and a 50/50 (vol/vol) mixture of F1 and F3. TDA experimental conditions: the same as in Figure 2. DLS experimental conditions: 10 mM PBS buffer, pH 7.4, η = 0.9×10^{-3} Pa.s. Sample: LNPs (DLin-MC3-DMA:DSPC:Chol:DMG-PEG-2000 at 50:10:40-x:x molar ratio) empty or encapsulating Firefly Luciferase (FLuc) mRNA. Sample dilution: 10 µL of the formulation into 1 mL PBS buffer. Temperature: 25°C. Measurement angle: 173°. Results presented in superposed triplicates.

Subsequently, TDA was used to study the degradation of mRNA in presence of RNase A. Figure 4A shows the analysis of mRNA diluted to 0.5 g/L in PBS buffer (without RNase A, see blue trace) giving an average hydrodynamic diameter of 43 nm. Repeating the same operation by adding a RNase A solution at 5 mg/L in PBS buffer (i.e. below RNase A detection limit in TDA) to the mRNA solution, led to much thinner peak (see green trace) and the hydrodynamic diameter was found only 1.4 nm. The same experiment was then carried out on an LNP formulation encapsulating mRNA. No significant difference in size was observed with or without the presence of RNase A, the hydrodynamic diameters being similar (82 and 84 nm, respectively). Finally, a 50/50 (vol/vol) mixture of a LNPs solution and a free (unencapsulated) mRNA solution was prepared. In the absence of RNase A, two size populations were observed, one of 43 nm corresponding to free mRNA and one of 84 nm corresponding to LNPs (see blue trace). In the presence of RNase A, a population of hydrodynamic diameter of 1.4 nm, corresponding to free mRNA degraded by RNase A, and another one of hydrodynamic diameter of 86 nm, corresponding to LNPs, were observed. The Gaussian fits of the elution profiles were presented in Figure S4. It is also interesting to note that after working with RNase A, an involuntary degradation of one Fluc mRNA sample was observed without voluntary addition of RNase A. The degradation, presented in Figure S5, was not immediate as observed for voluntary addition but evolved over time.

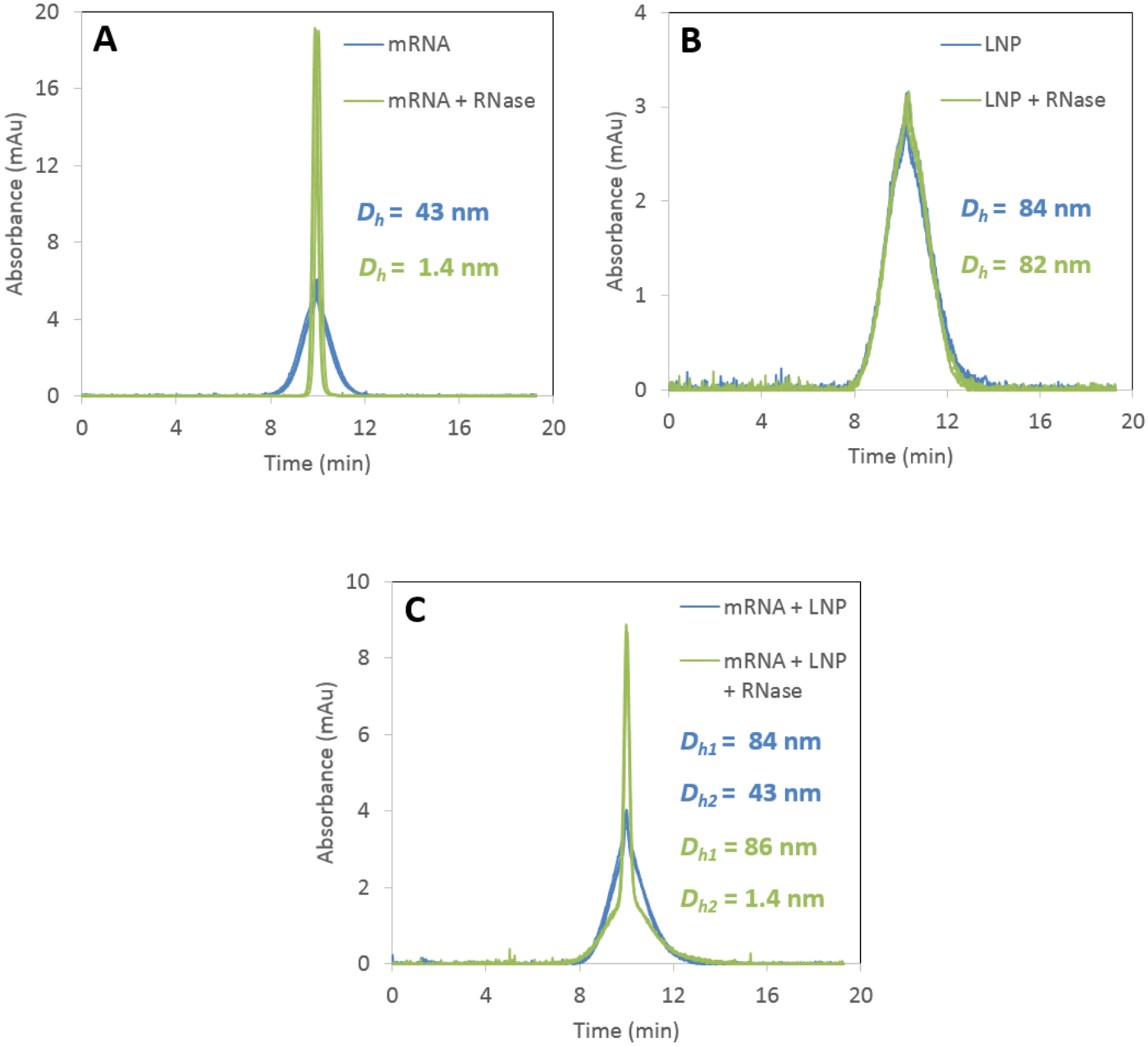

Figure 4: Taylorgrams obtained in the absence (blue trace) or in the presence (green trace) of RNase A for: free mRNA (A), LNPs formulation F2 (B) a mixture of free mRNA and LNPs formulation F2 (C). Experimental conditions: free mRNA: Firefly Luciferase (FLuc) mRNA, LNPs formulation: DLin-MC3-DMA:DSPC:Chol:DMG-PEG-2000 at 50:10:38.5:1.5 molar ratio encapsulating Firefly Luciferase (FLuc) mRNA. RNase A concentration in the final solutions 2.5 mg/L. Other conditions as in Figure 2. Results presented in superposed triplicates.

RiboGreen® Reagent was used with a fluorescence detector on the capillary electrophoresis equipment in order to access the integrity of the mRNA encapsulated within the LNPs and to calculate the encapsulation rate. This fluorescent reagent does not enter LNPs and allows to label only free mRNA (see red trace in Figure 5). LNPs were deformulated by adding a powerful surfactant Triton X-100 to access the amount of total mRNA (see purple trace in Figure 5). Comparing the free mRNA peaks obtained for the two formulations F1 and F3 in Figure 5, F1 was shown to have a lower level of encapsulation than F3. The ratio between the two peak areas (free mRNA/total mRNA) directly gave access to the degree of encapsulation. An encapsulation rate of 79% and 95% was obtained for F1 and F3, respectively. To confirm these results, the encapsulation efficiencies of the two formulations were also calculated by Ribogreen assay using SpectraMax® i3k. This orthogonal method gave similar encapsulation rates (75% and 94% for F1 and F3, respectively).

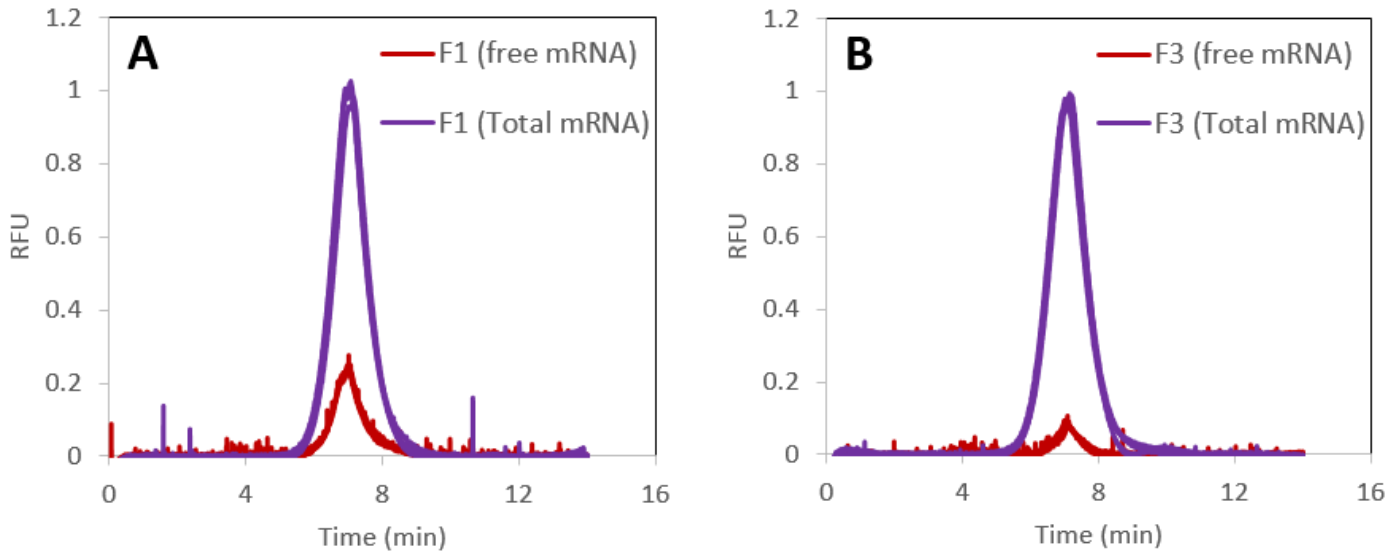

Figure 5: Taylorgrams obtained for the calculation of mRNA encapsulation rate and free mRNA hydrodynamic diameters for formulation F1 (A) and formulation F3 (B). Use of RiboGreen® fluorescent Reagent to label the free (unencapsulated) mRNA (red trace) and the total mRNA after deformulation of

the LNPs with Triton X-100 (purple trace). Experimental conditions: µSIL-FC coated capillaries of 61 cm total length (40 cm to the fluorescence detector) × 50 µm i.d. Buffer: TE buffer (10 mM Tris-HCl, 1 mM EDTA, pH 7.5). Capillary presaturation: LNPs for 10 min at 60 mbar. Capillary preconditioning: H_2O for 2 min at 960 mbar followed by 2 min TE buffer at 960 mbar. Injection: 20 mbar, 6 s. Mobilization pressure: 60 mbar. Sample: LNPs formulation F1 and F3 with RiboGreen® fluorescent Reagent and with (purple trace) or without (red trace) Triton X-100. Fluorescence detection excitation/emission: 480/520 nm. Results presented in superposed triplicates.

In parallel, it was possible to access the size of the mRNA, giving information on its integrity, by fitting the elution peaks. In the case of formulation F1, the average hydrodynamic diameter was 28 nm and 37 nm for the free mRNA and the total mRNA, respectively. In the case of formulation F2, the average hydrodynamic diameter was 10 nm and 42 nm for the free mRNA and the total mRNA, respectively.

Finally, using calibration curves performed with free mRNA, as presented in Figure S6, it was possible to access the concentration of the total mRNA and free mRNA present in one formulation. 12.3 µg/mL free mRNA and 60.7µg/mL total mRNA were found for formulation F1 and 3.2 µg/mL free mRNA and 62.1µg/mL total mRNA were found for formulation F3.

Discussion

The size of LNPs is a critical parameter for cellular uptake.[32,33] In this work, three parameters impacting LNPs size were studied. First, the PEG-lipid ratio was shown to have a significant impact on the size of LNPs, as a decrease from 5% to 0.5% multiplies the hydrodynamic diameter by 4. The strong influence of the PEG-lipid ratio has already been reported in the literature and the results obtained are in agreement with those of Belliveau et al.[34] and Yanez Arteta et al.[35] Furthermore, Bao et al.[36] showed that LNPs with higher PEG-C-DMA amount altered gene silencing efficacy by potentially reducing endosomal disruption. In addition, several studies reported the presence of anti-PEG antibodies[37,38], therefore the development of

new strategies to optimize or replace the PEG-lipid were explored.[39–43] But its replacement is tricky and other strategies must be considered for size optimization, especially trying to obtain small LNPs.

Two other parameters of the formulation that have also been reported to have an impact on LNPs size[44], were studied, namely the TFR and the FRR. It appeared that the higher the TFR and the FRR, the smaller the LNPs size. The faster the dilution of the ethanol phase in the aqueous phase, the less the time needed for lipids to group and stabilize, and the smaller the LNPs size. Therefore, the system used for mixing the organic and the aqueous phases is also a critical point for the production of LNPs of a defined size. To obtain small LNPs of well-defined size, the system must allow a rapid and homogeneous dilution of the ethanolic phase into the aqueous phase by maximizing the contact interface between the two fluids.[45,46]

The sizes, size distributions and polydispersity indices of the LNPs formulations measured by TDA using CRLI fit[47] were then compared to the ones obtained by DLS using Cumulant fit. The size distributions obtained by TDA were all narrower and less dragging towards large sizes than those obtained by DLS. Therefore, the mean hydrodynamic diameters and the polydispersity indices obtained by TDA were smaller than those one obtained by DLS. These differences can be explained by the fact that the two techniques do not determine the same size distributions. The size distribution obtained by TDA is related to the weight-average distribution, each LNP contributing to the distribution in proportion to their mass in the mixture. In contrast, the size distribution obtained by DLS is related to the intensity average distribution that gives more weight to the larger entities, since the distribution is weighted by the scattered intensity which scales as the hydrodynamic radius to the power 6. As the size distributions obtained by DLS are wider than by TDA, it is thus more difficult to distinguish two populations in DLS than in TDA. This was confirmed by the analysis of a mixture of two LNPs formulations

of different sizes. Indeed, DLS experiments showed single size distribution with an average size close to the one of the largest LNPs in the mixture, while TDA was able to identify the presence of two LNPs populations. These differences show the complementarity of the two methods in order to access LNPs accurate size. Moreover, the US FDA recommend the use of orthogonal methods to address technique-related differences for critical drug product parameters.[48]

Subsequently, TDA was used to study the degradation of mRNA in the presence of ribonucleases. Degradation of mRNA is one of the main reasons of why mRNA should be encapsulated into LNPs.[49,50] It was observed that the addition of small amounts of RNase A is able to cut mRNA into small pieces as its hydrodynamic diameter instantly drops from 43 to 1.4 nm. TDA thus allowed a clear observation of mRNA degradation. It is also interesting to note that after RNase A manipulation, all the elements brought into contact with RNase must be carefully cleaned, as we observed the day following the voluntary degradation tests, a non-voluntary degradation of one mRNA sample. As only traces of RNase were present, the degradation was in the latter case not immediate but more gradual. Concerning the LNPs, no visible degradation was observed by TDA after RNase addition.

Then, TDA was used to look into the encapsulation rate of mRNA within LNPs and the size integrity of the encapsulated mRNA. The results obtained were consistent with those obtained by Ribogreen assay using a microplate reader. The degree of encapsulation is an important parameter, as unencapsulated mRNA can easily be degraded and hardly penetrate into the cytoplasm of cells due to its negative charge. The mRNA integrity is also a critical parameter, as in case it is degraded, it can thus no longer be translated into the protein of interest. Therefore, the vaccine efficacy highly depends on the rate of encapsulation and on mRNA integrity.

Finally, this study showed that a single capillary electrophoresis equipment is able to provide much information on mRNA-LNPs formulations. As TDA is quick and easy to

automatize, it could be used both for quality control to check the correct progress of LNP formulation processes and for stability studies to check the absence of aggregation of LNPs and the mRNA size integrity. As it consumes little product, TDA can also be used for research purpose and could serve to optimize LNPs formulations parameters. Moreover, it allows to challenge existing analytical methods and the orthogonal use of different methods allow to have a more exact idea of the accurate size of LNPs. However, each method has its own limitations and the main one of TDA remains the adsorption of molecules on the capillary walls, requiring capillary coatings, presaturation steps and rinsing steps.

Materials and Methods

Chemicals and Materials. FLuc (Cyanine 5 Firefly Luciferase) mRNA (1929 nucleotides) at 1 mg/mL in 1 mM sodium citrate pH 6.4 was purchased from TriLink BioTechnologies (San Diego, CA, USA). RNase-free water DEPC treated was purchased from Thermo Fisher Scientific (Illkirch-Graffenstaden, France). Trisodium citrate dihydrate $HOC(COONa)(CH_2COONa)_2 \cdot 2H_2O$, ($M_w$ = 294.1 g/mol) and citric acid monohydrate $HOC(COOH)(CH_2COOH)_2 \cdot H_2O$ (M_w = 210.1 g/mol) were purchased from Merk (Darmstadt, Germany). DLin-MC3-DMA ((6Z,9Z,28Z,31Z)-heptatriacont-6,9,28,31-tetraene-19-yl 4-(dimethylamino)butanoate) was purchased from Sai Life Sciences Ltd. (Telangana, India). DSPC (1,2-distearoyl-sn-glycero-3-phosphocholine), Chol (cholesterol) and DMG-PEG-2000 (1,2-dimyristoyl-rac-glycero-3-methoxypolyethylene glycol-2000) were purchased from Sigma-Aldrich (St. Quentin Fallavier, France). Absolute ethanol was purchased from Carlo Erba Reagents (Val de Reuil, France). PBS (phosphate-buffered saline) 10X buffer was purchased from Eurobio Scientific (Les Ulis, France). Slide-A-Lyzer™ dialysis cassettes, 10K MWCO, 3 mL, were purchased from Thermo Fisher Scientific (Illkirch-Graffenstaden, France). µSIL-FC

(fluorocarbon polymer) coated capillaries were purchased from Agilent Technologies (Santa Clara, CA, USA). Invitrogen™ Quant-iT™ RiboGreen™ RNA Assay Kit and Pierce™ White Opaque 96-Well Plates were purchased from Thermo Fisher Scientific (Illkirch-Graffenstaden, France). Ribonuclease A from bovine pancreas (RNase A, M_w = 14 kDa, pI = 9) and Triton™ X-100 were purchased from Merk (Darmstadt, Germany). Deionized water was further purified with a Milli-Q system from Millipore (Molsheim, France).

Formulation of LNPs. Lipid nanoparticles (LNPs) self-assemble by the rapid dilution of an organic phase containing lipids in a mRNA containing aqueous phase. The organic phase was prepared by mixing the 4 lipids in absolute ethanol at the following molar ratio DLinMC3-DMA:DSPC:Chol:DMG-PEG-2000 (50:10:40-x:x). Stock solutions of lipids were previously prepared in absolute ethanol at the following concentrations: DLinMC3-DMA 100 mg/mL, DSPC 30 mg/mL, Chol 18 mg/mL, DMG-PEG-2000 30 mg/mL. The aqueous phase was prepared by diluting mRNA at 0.25 g/L in 50 mM RNase free citrate buffer, pH 4. The mixing step was performed using NanoAssemblr® instrument from Precision NanoSystems (Vancouver, Canada). One syringe was filled with the aqueous solution and another one with the ethanolic solution. LNPs are then produced setting up the NanoAssemblr® software with the following parameters: Flow Rate Ratio (FRR) and Total Flow Rate (TFR). Both parameters varied according to each formulation, as explained in the Results section. 2 mL solution were involved per formulation with 0.45 mL of start waste volume and 0.05 mL of end waste volume, resulting in 1.5 mL per LNP formulation. After formulation, each LNP formulation was immediately dialyzed one night against 500 mL of 50 mM citrate buffer, pH 4 using Slide-A-Lyzer dialysis cassette 10K MWCO. This first dialysis was performed to remove residual ethanol. After that, two successive dialysis of one day and one night long in total were performed against 500 mL PBS buffer at pH 7.4 to raise the pH to physiological value. The size of the different LNPs

formulations was then determined by DLS and the formulations were filtered using 0.2 or 0.45 micrometer filters according to their size.

Taylor Dispersion Analysis (TDA). The equipment used for TDA experiments was a 7100 Capillary Electrophoresis Agilent system (Waldbronn, Germany). This system was equipped with a diode array detector (DAD) and with a Zetalif LED induced fluorescence (LEDIF) detector purchased from Adelis (Grabels, France), both connected in series. The UV measurements were performed at 200 nm. The fluorescent measurements were performed with excitation at 640 nm (for Cyanine 5 labelled mRNA) or 480 nm (for RiboGreen® RNA dye). The temperature of the capillary cartridge was set at 25°C. The LNPs formulations were injected without prior dilution into the capillaries filled with PBS buffer. TDA experiments were performed using 60 mbar mobilization pressure of a sample plug injected at 20 mbar for 6 s. The elution peaks obtained were fitted using one or two Gaussians, depending on the number of objects in the solution, according to equation (1) using a home-developed Excel spreadsheet :

$$S(t) = \sum_{i=1}^{2} \frac{A_i}{\sigma_i \sqrt{2\pi}} exp \frac{-(t-t_0)^2}{2{\sigma_i}^2} \quad (1)$$

where $S(t)$ is the absorbance signal, σ_i is the temporal variance, A_i is a constant that depended on the response factor and the injected quantity of solute and t_0 is the average elution time. t_0 is directly obtained from the position of the maximum of absorbance and σ_i, and A_i are adjusting parameters obtained by nonlinear least square regression using Excel solver.

The temporal variance σ_i allows to calculate the molecular diffusion coefficient D_i according to equation (2):

$$D_i = \frac{R_c^2 t_0}{24{\sigma_i}^2} \quad (2)$$

where R_c is the capillary radius. Stokes–Einstein equation (3) allows then to determine the hydrodynamic diameter $D_{h,i}$:

$$D_{h,i} = \frac{k_B T}{6\pi\eta D_i} \quad (3)$$

where k_B is the Boltzmann constant, T is the temperature, and η is the eluent viscosity.

To get the size distribution, the elution profile can be fitted using a second approach based on Regularized Linear Inversion (CRLI) algorithm[31] according to equation (4):

$$S(t) = \int_0^\infty CM(D)\rho(D)\sqrt{D}\, exp\left[\frac{-(t-t_0)^2 12D}{{R_c}^2 t_0}\right] dD \quad (4)$$

where C is an instrumental constant, $M(D)$ and $\rho(D)$ are the mass and the molar concentration of the objects with the diffusion coefficient D, respectively. The polydispersity of the sample can further be determined using equations (5) and (6):

$${\sigma_{D_h}}^2 = \frac{\int_{D_{hmin}}^{D_{hmax}} (D_h - \overline{D_h})^2 P(D_h) dD_h}{\int_{D_{hmin}}^{D_{hmax}} P(D_h) dD_h} \quad (5)$$

$$PDI = \left(\frac{\sigma_{D_h}}{\overline{D_h}}\right)^2 \quad (6)$$

Dynamic Light Scattering (DLS). The equipment used for DLS experiments was a Malvern Panalytical Zetasizer Nano ZS system (Palaiseau, France). LNPs formulations were diluted by adding 10 µL of the formulation into 1 mL PBS buffer. The temperature of the cuvettes was set at 25°C. The measurement angle was 173°. Cumulant fit was used to fit the experimental data of the autocorrelation function.

Encapsulation efficiency by Ribogreen assay. To determine mRNA encapsulation efficiency, two calibration curves were first performed with unformulated mRNA. The first curve was determined with mRNA diluted in 1X RNase free TE buffer and the second

one in 1X RNase free TE buffer with 0.5% (v/v) Trition X-100 in a 96-well plate. Quant-iT RiboGreen fluorescent reagent was then added to each well and the fluorescence signal (excitation/emission: 480/520 nm) was quantified using SpectraMax® i3k from Molecular Devices (San Jose, CA, USA).

LNP-mRNA formulations were then also diluted in 1X RNase free TE buffer and in 1X RNase free TE buffer with 0.5% (v/v) Trition X-100, followed by Quant-iT RiboGreen reagent addition. mRNA encapsulation was determined by comparing the fluorescence in the presence and in the absence of Triton X-100. In the absence of Triton X-100, the signal only comes from the free (unencapsulated) mRNA while, in the presence of Triton X-100, the signal comes from the total mRNA as the detergent allows to break the LNPs. The encapsulation efficiencies (ee%) were therefore calculated according to equation (7):

$$ee\% = \left(1 - \frac{free\ mRNA\ (without\ Triton)}{total\ mRNA\ (with\ Triton)}\right) \times 100 \qquad (7)$$

Acknowledgments

This work was partly funded by Sanofi Pasteur under a Cooperative Research and Development Agreement with the University of Montpellier and the CNRS.

Author Contributions

C. M., L. L., J-F. C., J. T., and H. C. designed this study. C. M. and E. B. formulated the LNPs. C.M. performed the TDA and DLS experiments. L. L., J-F. C., J. T., E. B., M. G. and H. C. reviewed the data. C.M. wrote the manuscript. L. L., J-F. C., J. T., E. B., M. G. and H. C. reviewed and edited the manuscript.

References

(1) Rappuoli, R.; Pizza, M.; Del Giudice, G.; De Gregorio, E. Vaccines, New Opportunities for a New Society. *Proc. Natl. Acad. Sci.* **2014**, *111* (34), 12288–12293. https://doi.org/10.1073/pnas.1402981111.

(2) Pollard, A. J.; Bijker, E. M. A Guide to Vaccinology: From Basic Principles to New Developments. *Nat. Rev. Immunol.* **2021**, *21* (2), 83–100. https://doi.org/10.1038/s41577-020-00479-7.

(3) Morens, D. M.; Fauci, A. S. Emerging Pandemic Diseases: How We Got to COVID-19. *Cell* **2020**, *182* (5), 1077–1092. https://doi.org/10.1016/j.cell.2020.08.021.

(4) Hajj, K. A.; Whitehead, K. A. Tools for Translation: Non-Viral Materials for Therapeutic MRNA Delivery. *Nat. Rev. Mater.* **2017**, *2* (10), 17056. https://doi.org/10.1038/natrevmats.2017.56.

(5) Nanomedicine and the COVID-19 Vaccines. *Nat. Nanotechnol.* **2020**, *15* (12), 963–963. https://doi.org/10.1038/s41565-020-00820-0.

(6) Wolff, J.; Malone, R.; Williams, P.; Chong, W.; Acsadi, G.; Jani, A.; Felgner, P. Direct Gene Transfer into Mouse Muscle in Vivo. *Science* **1990**, *247* (4949), 1465–1468. https://doi.org/DOI:10.1126/science.1690918.

(7) Pardi, N.; Hogan, M. J.; Porter, F. W.; Weissman, D. MRNA Vaccines — a New Era in Vaccinology. *Nat. Rev. Drug Discov.* **2018**, *17* (4), 261–279. https://doi.org/10.1038/nrd.2017.243.

(8) Guan, S.; Rosenecker, J. Nanotechnologies in Delivery of MRNA Therapeutics Using Nonviral Vector-Based Delivery Systems. *Gene Ther.* **2017**, *24* (3), 133–143. https://doi.org/10.1038/gt.2017.5.

(9) Zhang, X.; Goel, V.; Robbie, G. J. Pharmacokinetics of Patisiran, the First Approved RNA Interference Therapy in Patients With Hereditary Transthyretin-Mediated Amyloidosis. *J. Clin. Pharmacol.* **2020**, *60* (5), 573–585. https://doi.org/10.1002/jcph.1553.

(10) Urits, I.; Swanson, D.; Swett, M. C.; Patel, A.; Berardino, K.; Amgalan, A.; Berger, A. A.; Kassem, H.; Kaye, A. D.; Viswanath, O. A Review of Patisiran (ONPATTRO®) for the Treatment of Polyneuropathy in People with Hereditary Transthyretin Amyloidosis. *Neurol. Ther.* **2020**, *9* (2), 301–315. https://doi.org/10.1007/s40120-020-00208-1.

(11) Akinc, A.; Maier, M. A.; Manoharan, M.; Fitzgerald, K.; Jayaraman, M.; Barros, S.; Ansell, S.; Du, X.; Hope, M. J.; Madden, T. D.; Mui, B. L.; Semple, S. C.; Tam, Y. K.; Ciufolini, M.; Witzigmann, D.; Kulkarni, J. A.; van der Meel, R.; Cullis, P. R. The Onpattro Story and the Clinical Translation of Nanomedicines Containing Nucleic Acid-Based Drugs. *Nat. Nanotechnol.* **2019**, *14* (12), 1084–1087. https://doi.org/10.1038/s41565-019-0591-y.

(12) Kim, Y. C.; Dema, B.; Reyes-Sandoval, A. COVID-19 Vaccines: Breaking Record Times to First-in-Human Trials. *Npj Vaccines* **2020**, *5* (1), 34. https://doi.org/10.1038/s41541-020-0188-3.

(13) Friedrichs, S.; Bowman, D. M. COVID-19 May Become Nanomedicine's Finest Hour yet. *Nat. Nanotechnol.* **2021**, *16* (4), 362–364. https://doi.org/10.1038/s41565-021-00901-8.

(14) Schoenmaker, L.; Witzigmann, D.; Kulkarni, J. A.; Verbeke, R.; Kersten, G.; Jiskoot, W.; Crommelin, D. J. A. MRNA-Lipid Nanoparticle COVID-19 Vaccines: Structure and Stability. *Int. J. Pharm.* **2021**, *601*, 120586. https://doi.org/10.1016/j.ijpharm.2021.120586.
(15) Crommelin, D. J. A.; Anchordoquy, T. J.; Volkin, D. B.; Jiskoot, W.; Mastrobattista, E. Addressing the Cold Reality of MRNA Vaccine Stability. *J. Pharm. Sci.* **2021**, *110* (3), 997–1001. https://doi.org/10.1016/j.xphs.2020.12.006.
(16) Gilleron, J.; Querbes, W.; Zeigerer, A.; Borodovsky, A.; Marsico, G.; Schubert, U.; Manygoats, K.; Seifert, S.; Andree, C.; Stöter, M.; Epstein-Barash, H.; Zhang, L.; Koteliansky, V.; Fitzgerald, K.; Fava, E.; Bickle, M.; Kalaidzidis, Y.; Akinc, A.; Maier, M.; Zerial, M. Image-Based Analysis of Lipid Nanoparticle–Mediated SiRNA Delivery, Intracellular Trafficking and Endosomal Escape. *Nat. Biotechnol.* **2013**, *31* (7), 638–646. https://doi.org/10.1038/nbt.2612.
(17) Sabnis, S.; Kumarasinghe, E. S.; Salerno, T.; Mihai, C.; Ketova, T.; Senn, J. J.; Lynn, A.; Bulychev, A.; McFadyen, I.; Chan, J.; Almarsson, Ö.; Stanton, M. G.; Benenato, K. E. A Novel Amino Lipid Series for MRNA Delivery: Improved Endosomal Escape and Sustained Pharmacology and Safety in Non-Human Primates. *Mol. Ther.* **2018**, *26* (6), 1509–1519. https://doi.org/10.1016/j.ymthe.2018.03.010.
(18) Cheng, Q.; Wei, T.; Farbiak, L.; Johnson, L. T.; Dilliard, S. A.; Siegwart, D. J. Selective Organ Targeting (SORT) Nanoparticles for Tissue-Specific MRNA Delivery and CRISPR–Cas Gene Editing. *Nat. Nanotechnol.* **2020**, *15* (4), 313–320. https://doi.org/10.1038/s41565-020-0669-6.
(19) Dammes, N.; Goldsmith, M.; Ramishetti, S.; Dearling, J. L. J.; Veiga, N.; Packard, A. B.; Peer, D. Conformation-Sensitive Targeting of Lipid Nanoparticles for RNA Therapeutics. *Nat. Nanotechnol.* **2021**. https://doi.org/10.1038/s41565-021-00928-x.
(20) Wilhelm, S.; Tavares, A. J.; Dai, Q.; Ohta, S.; Audet, J.; Dvorak, H. F.; Chan, W. C. W. Analysis of Nanoparticle Delivery to Tumours. *Nat. Rev. Mater.* **2016**, *1* (5), 16014. https://doi.org/10.1038/natrevmats.2016.14.
(21) Jiang, W.; Kim, B. Y. S.; Rutka, J. T.; Chan, W. C. W. Nanoparticle-Mediated Cellular Response Is Size-Dependent. *Nat. Nanotechnol.* **2008**, *3* (3), 145–150. https://doi.org/10.1038/nnano.2008.30.
(22) Conner, S. D.; Schmid, S. L. Regulated Portals of Entry into the Cell. *Nature* **2003**, *422* (6927), 37–44. https://doi.org/10.1038/nature01451.
(23) Rejman, J.; Oberle, V.; Zuhorn, I. S.; Hoekstra, D. Size-Dependent Internalization of Particles via the Pathways of Clathrin- and Caveolae-Mediated Endocytosis. *Biochem. J.* **2004**, *377* (Pt 1), 159–169. https://doi.org/10.1042/BJ20031253.
(24) Petros, R. A.; DeSimone, J. M. Strategies in the Design of Nanoparticles for Therapeutic Applications. *Nat. Rev. Drug Discov.* **2010**, *9* (8), 615–627. https://doi.org/10.1038/nrd2591.
(25) Andar, A. U.; Hood, R. R.; Vreeland, W. N.; DeVoe, D. L.; Swaan, P. W. Microfluidic Preparation of Liposomes to Determine Particle Size Influence on Cellular Uptake Mechanisms. *Pharm. Res.* **2014**, *31* (2), 401–413. https://doi.org/10.1007/s11095-013-1171-8.
(26) Evers, M. J. W.; Kulkarni, J. A.; van der Meel, R.; Cullis, P. R.; Vader, P.; Schiffelers, R. M. State-of-the-Art Design and Rapid-Mixing Production

Techniques of Lipid Nanoparticles for Nucleic Acid Delivery. *Small Methods* **2018**, *2* (9), 1700375. https://doi.org/10.1002/smtd.201700375.
(27) Chauhan, V. P.; Jain, R. K. Strategies for Advancing Cancer Nanomedicine. *Nat. Mater.* **2013**, *12* (11), 958–962. https://doi.org/10.1038/nmat3792.
(28) Le-Vinh, B.; Steinbring, C.; Wibel, R.; Friedl, J. D.; Bernkop-Schnürch, A. Size Shifting of Solid Lipid Nanoparticle System Triggered by Alkaline Phosphatase for Site Specific Mucosal Drug Delivery. *Eur. J. Pharm. Biopharm.* **2021**, *163*, 109–119. https://doi.org/10.1016/j.ejpb.2021.03.012.
(29) Trevaskis, N. L.; Kaminskas, L. M.; Porter, C. J. H. From Sewer to Saviour — Targeting the Lymphatic System to Promote Drug Exposure and Activity. *Nat. Rev. Drug Discov.* **2015**, *14* (11), 781–803. https://doi.org/10.1038/nrd4608.
(30) Fan, Y.; Marioli, M.; Zhang, K. Analytical Characterization of Liposomes and Other Lipid Nanoparticles for Drug Delivery. *J. Pharm. Biomed. Anal.* **2021**, *192*, 113642. https://doi.org/10.1016/j.jpba.2020.113642.
(31) Cipelletti, L.; Biron, J.-P.; Martin, M.; Cottet, H. Measuring Arbitrary Diffusion Coefficient Distributions of Nano-Objects by Taylor Dispersion Analysis. *Anal. Chem.* **2015**, *87* (16), 8489–8496. https://doi.org/10.1021/acs.analchem.5b02053.
(32) Mitchell, M. J.; Billingsley, M. M.; Haley, R. M.; Wechsler, M. E.; Peppas, N. A.; Langer, R. Engineering Precision Nanoparticles for Drug Delivery. *Nat. Rev. Drug Discov.* **2021**, *20* (2), 101–124. https://doi.org/10.1038/s41573-020-0090-8.
(33) Zhang, S.; Li, J.; Lykotrafitis, G.; Bao, G.; Suresh, S. Size-Dependent Endocytosis of Nanoparticles. *Adv. Mater.* **2009**, *21* (4), 419–424. https://doi.org/10.1002/adma.200801393.
(34) Belliveau, N. M.; Huft, J.; Lin, P. J.; Chen, S.; Leung, A. K.; Leaver, T. J.; Wild, A. W.; Lee, J. B.; Taylor, R. J.; Tam, Y. K.; Hansen, C. L.; Cullis, P. R. Microfluidic Synthesis of Highly Potent Limit-Size Lipid Nanoparticles for In Vivo Delivery of SiRNA. *Mol. Ther. - Nucleic Acids* **2012**, *1*, e37. https://doi.org/10.1038/mtna.2012.28.
(35) Yanez Arteta, M.; Kjellman, T.; Bartesaghi, S.; Wallin, S.; Wu, X.; Kvist, A. J.; Dabkowska, A.; Székely, N.; Radulescu, A.; Bergenholtz, J.; Lindfors, L. Successful Reprogramming of Cellular Protein Production through MRNA Delivered by Functionalized Lipid Nanoparticles. *Proc. Natl. Acad. Sci.* **2018**, *115* (15), E3351. https://doi.org/10.1073/pnas.1720542115.
(36) Bao, Y.; Jin, Y.; Chivukula, P.; Zhang, J.; Liu, Y.; Liu, J.; Clamme, J.-P.; Mahato, R. I.; Ng, D.; Ying, W.; Wang, Y.; Yu, L. Effect of PEGylation on Biodistribution and Gene Silencing of SiRNA/Lipid Nanoparticle Complexes. *Pharm. Res.* **2013**, *30* (2), 342–351. https://doi.org/10.1007/s11095-012-0874-6.
(37) Kozma, G. T.; Shimizu, T.; Ishida, T.; Szebeni, J. Anti-PEG Antibodies: Properties, Formation, Testing and Role in Adverse Immune Reactions to PEGylated Nano-Biopharmaceuticals. *Adv. Liposome Res.* **2020**, *154–155*, 163–175. https://doi.org/10.1016/j.addr.2020.07.024.
(38) Hoang Thi, T. T.; Pilkington, E. H.; Nguyen, D. H.; Lee, J. S.; Park, K. D.; Truong, N. P. The Importance of Poly(Ethylene Glycol) Alternatives for Overcoming PEG Immunogenicity in Drug Delivery and Bioconjugation. *Polymers* **2020**, *12* (2), 298. https://doi.org/10.3390/polym12020298.
(39) Nogueira, S. S.; Schlegel, A.; Maxeiner, K.; Weber, B.; Barz, M.; Schroer, M. A.; Blanchet, C. E.; Svergun, D. I.; Ramishetti, S.; Peer, D.; Langguth, P.; Sahin, U.;

Haas, H. Polysarcosine-Functionalized Lipid Nanoparticles for Therapeutic MRNA Delivery. *ACS Appl. Nano Mater.* **2020**, *3* (11), 10634–10645. https://doi.org/10.1021/acsanm.0c01834.
(40) Joh, D. Y.; Zimmers, Z.; Avlani, M.; Heggestad, J. T.; Aydin, H. B.; Ganson, N.; Kumar, S.; Fontes, C. M.; Achar, R. K.; Hershfield, M. S.; Hucknall, A. M.; Chilkoti, A. Architectural Modification of Conformal PEG-Bottlebrush Coatings Minimizes Anti-PEG Antigenicity While Preserving Stealth Properties. *Adv. Healthc. Mater.* **2019**, *8* (8), 1801177. https://doi.org/10.1002/adhm.201801177.
(41) Ou, H.; Cheng, T.; Zhang, Y.; Liu, J.; Ding, Y.; Zhen, J.; Shen, W.; Xu, Y.; Yang, W.; Niu, P.; Liu, J.; An, Y.; Liu, Y.; Shi, L. Surface-Adaptive Zwitterionic Nanoparticles for Prolonged Blood Circulation Time and Enhanced Cellular Uptake in Tumor Cells. *Acta Biomater.* **2018**, *65*, 339–348. https://doi.org/10.1016/j.actbio.2017.10.034.
(42) Pitek, A. S.; Jameson, S. A.; Veliz, F. A.; Shukla, S.; Steinmetz, N. F. Serum Albumin 'Camouflage' of Plant Virus Based Nanoparticles Prevents Their Antibody Recognition and Enhances Pharmacokinetics. *Biomaterials* **2016**, *89*, 89–97. https://doi.org/10.1016/j.biomaterials.2016.02.032.
(43) Gulati, N. M.; Stewart, P. L.; Steinmetz, N. F. Bioinspired Shielding Strategies for Nanoparticle Drug Delivery Applications. *Mol. Pharm.* **2018**, *15* (8), 2900–2909. https://doi.org/10.1021/acs.molpharmaceut.8b00292.
(44) Roces, C. B.; Lou, G.; Jain, N.; Abraham, S.; Thomas, A.; Halbert, G. W.; Perrie, Y. Manufacturing Considerations for the Development of Lipid Nanoparticles Using Microfluidics. *Pharmaceutics* **2020**, *12* (11). https://doi.org/10.3390/pharmaceutics12111095.
(45) Zhigaltsev, I. V.; Belliveau, N.; Hafez, I.; Leung, A. K. K.; Huft, J.; Hansen, C.; Cullis, P. R. Bottom-Up Design and Synthesis of Limit Size Lipid Nanoparticle Systems with Aqueous and Triglyceride Cores Using Millisecond Microfluidic Mixing. *Langmuir* **2012**, *28* (7), 3633–3640. https://doi.org/10.1021/la204833h.
(46) Chiesa, E.; Greco, A.; Riva, F.; Tosca, E. M.; Dorati, R.; Pisani, S.; Modena, T.; Conti, B.; Genta, I. Staggered Herringbone Microfluid Device for the Manufacturing of Chitosan/TPP Nanoparticles: Systematic Optimization and Preliminary Biological Evaluation. *Int. J. Mol. Sci.* **2019**, *20* (24), 6212. https://doi.org/10.3390/ijms20246212.
(47) Cipelletti, L.; Biron, J.-P.; Martin, M.; Cottet, H. Measuring Arbitrary Diffusion Coefficient Distributions of Nano-Objects by Taylor Dispersion Analysis. *Anal. Chem.* **2015**, *87* (16), 8489–8496. https://doi.org/10.1021/acs.analchem.5b02053.
(48) U.S. FDA. Drug Products, Including Biological Products, That Contain Nanomaterials-Guidance for Industry. 2017.
(49) Let's Talk about Lipid Nanoparticles. *Nat. Rev. Mater.* **2021**, *6* (2), 99–99. https://doi.org/10.1038/s41578-021-00281-4.
(50) Reichmuth, A. M.; Oberli, M. A.; Jaklenec, A.; Langer, R.; Blankschtein, D. MRNA Vaccine Delivery Using Lipid Nanoparticles. *Ther. Deliv.* **2016**, *7* (5), 319–334. https://doi.org/10.4155/tde-2016-0006.